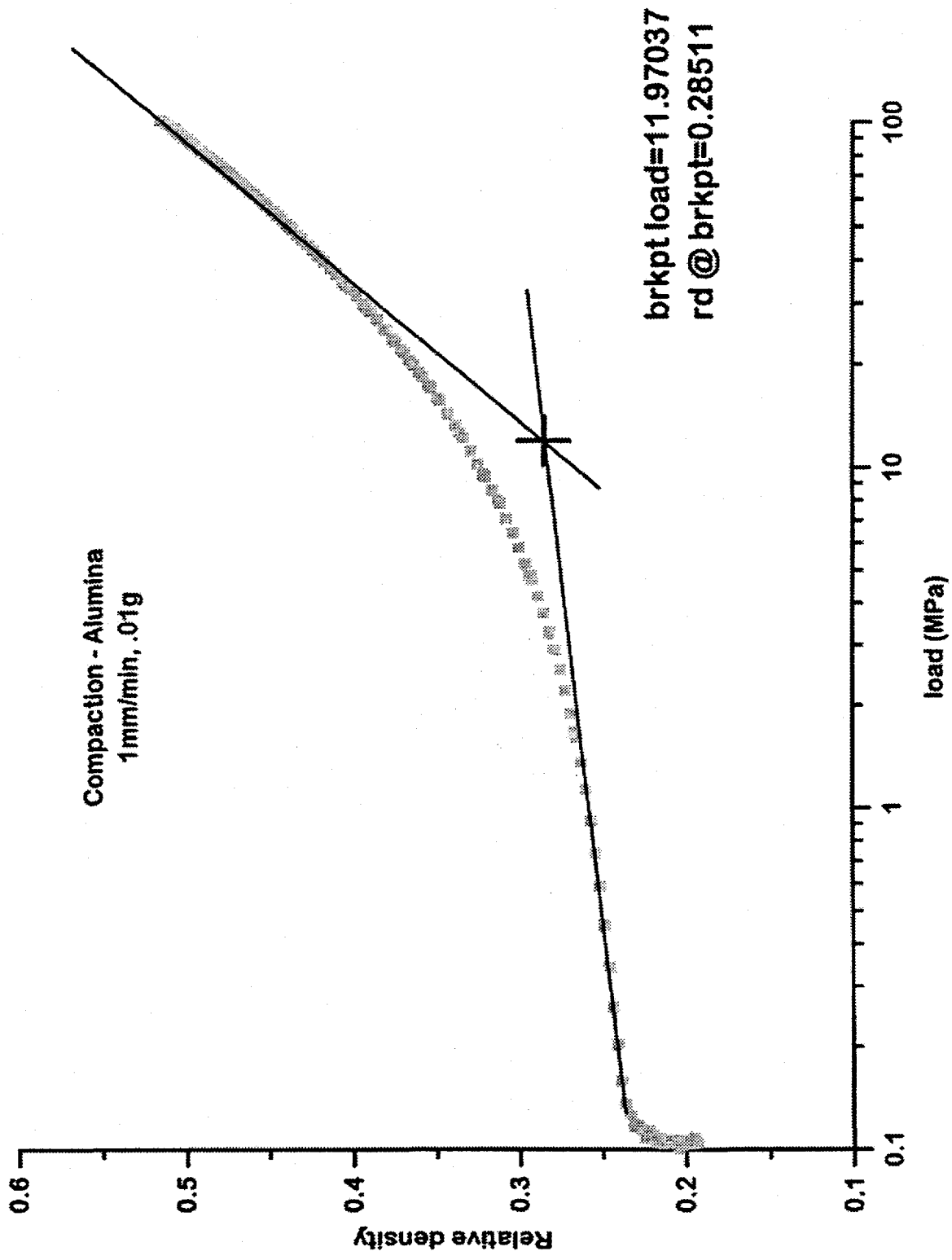

Fig. 1 Uniaxial compaction results for the Vista alumina sample VISTA-B-965-500C obtained from Dr. Robert Gormley. The relative density vs log P curve can be fit by two linear segments whose intersection determines a nominal breaking strength (11.97 MPa) for the alumina granules.

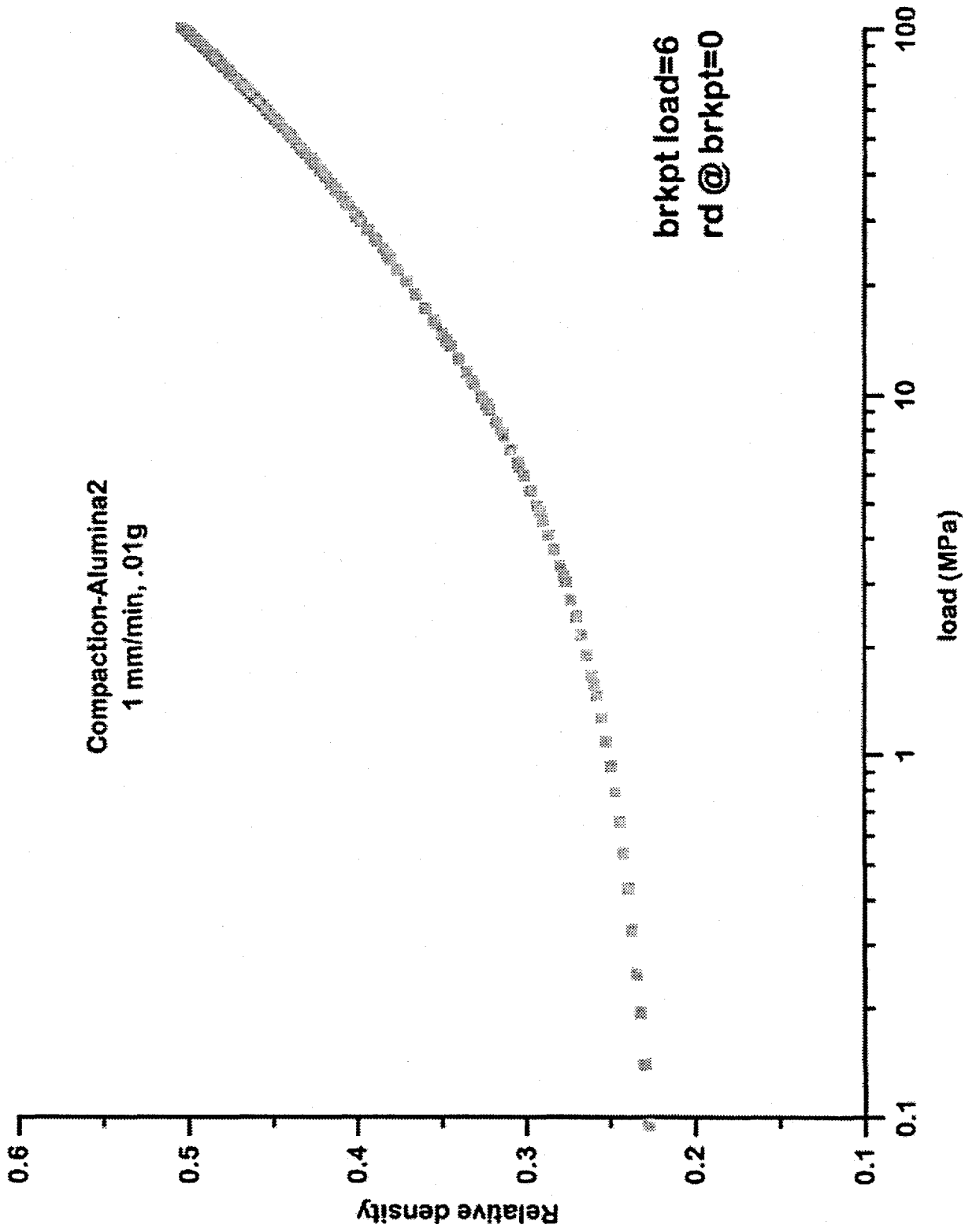

Fig. 2 Uniaxial compaction results for a second aliquot of the same alumina sample shown in Fig. 1. The compaction curve up to a pressure of 30MPa is very similar to that of fig. 1, however, using linear fits to the data at low and high pressures yields a breakpoint of 6 MPa.

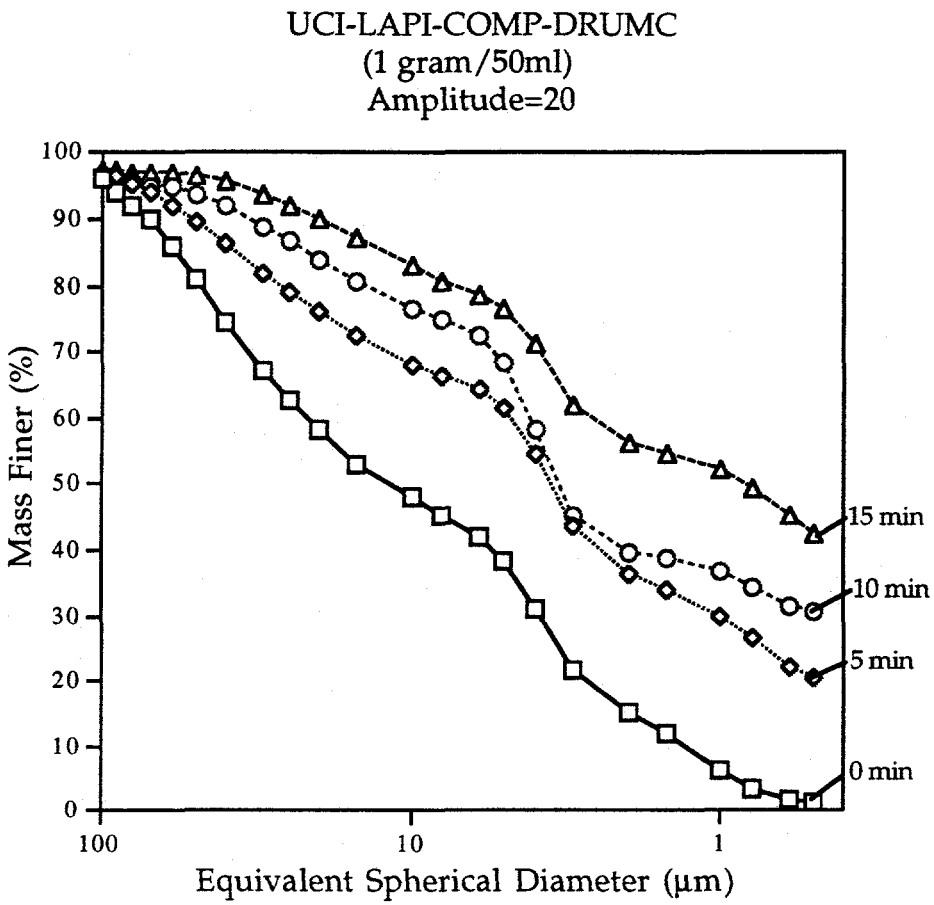

Fig. 3 Sedigraph particle size measurements for UCI F-T catalyst UCI-LAPI-COMP-DRUMC. The abscissa represents mass % of the sample finer than the indicated equivalent diameter. The sample represents a composite catalyst from the batch prepared for LaPorte run I. As seen from this figure, 15 minutes of ultrasound at a level of 20 causes considerable particle breakdown and generation of fine particles.

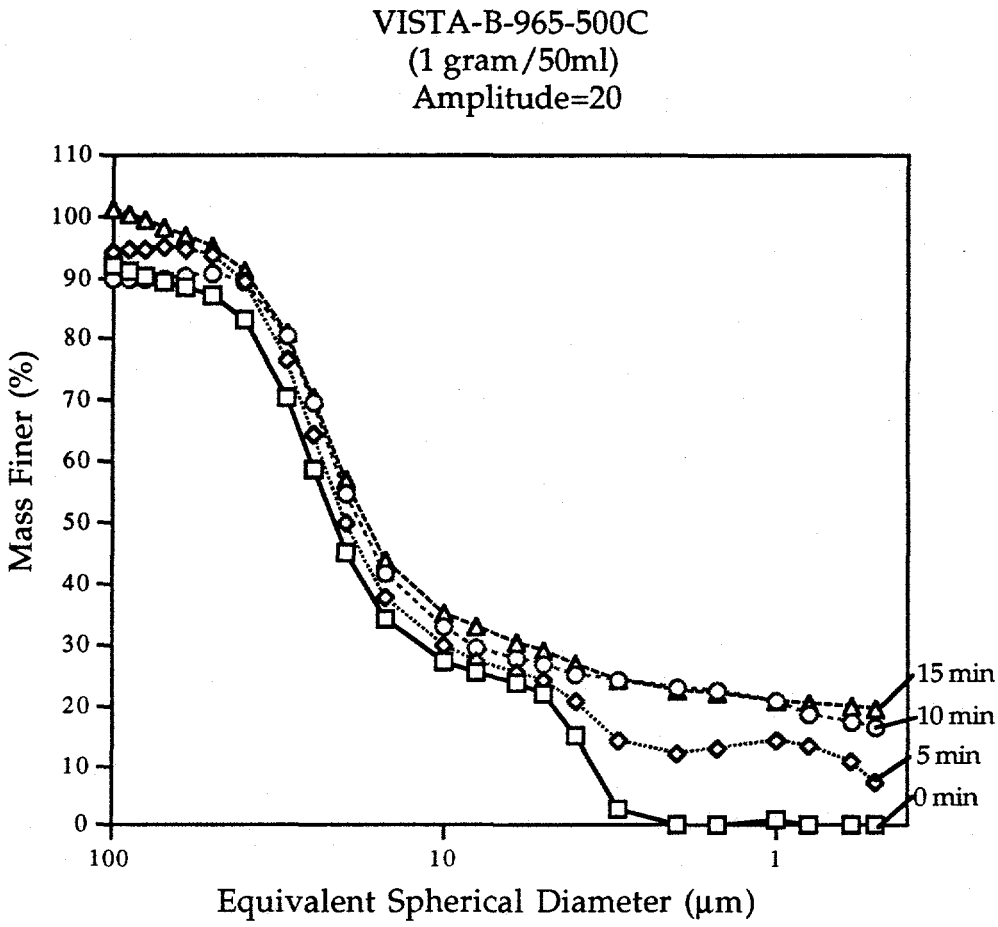

Fig. 4 Sedigraph particle size distribution of sample VISTA-B-965-500C obtained from Dr. RObert Gormley. The starting alumina from Vista was sieved and calcined in air at 500 °C. As seen from this figure, the alumina granules are much stronger than the catalyst shown in Fig. 3 and show very little fragmentation after 15 min of ultrasound irradiation.

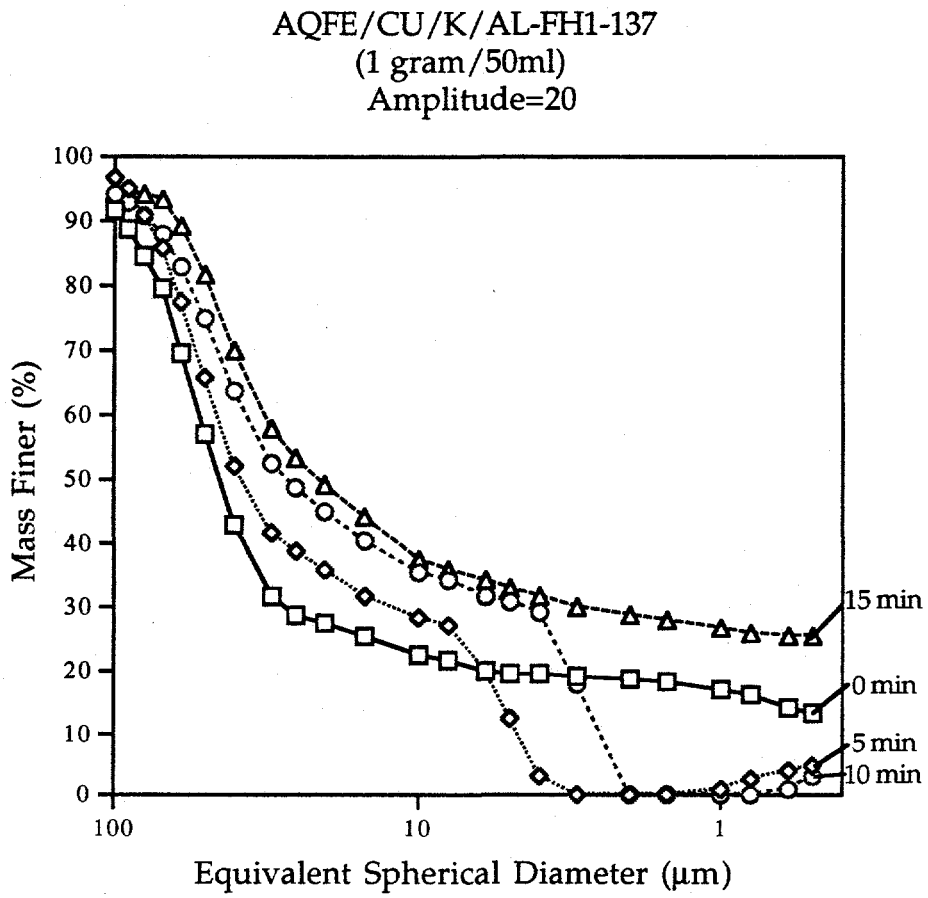

Fig. 5 Sedigraph particle size distributions of catalyst AQFE/CU/K/AL-FH1-137 which was prepared by Dr. Robert Gormley at PETC by impregnation of the Vista alumina (shown in Fig. 4). There appears to be some irreproducibility in the results with particles smaller than 10 μm. However, the extent of particle breakdown appears to be only marginally greater than the blank alumina sample.

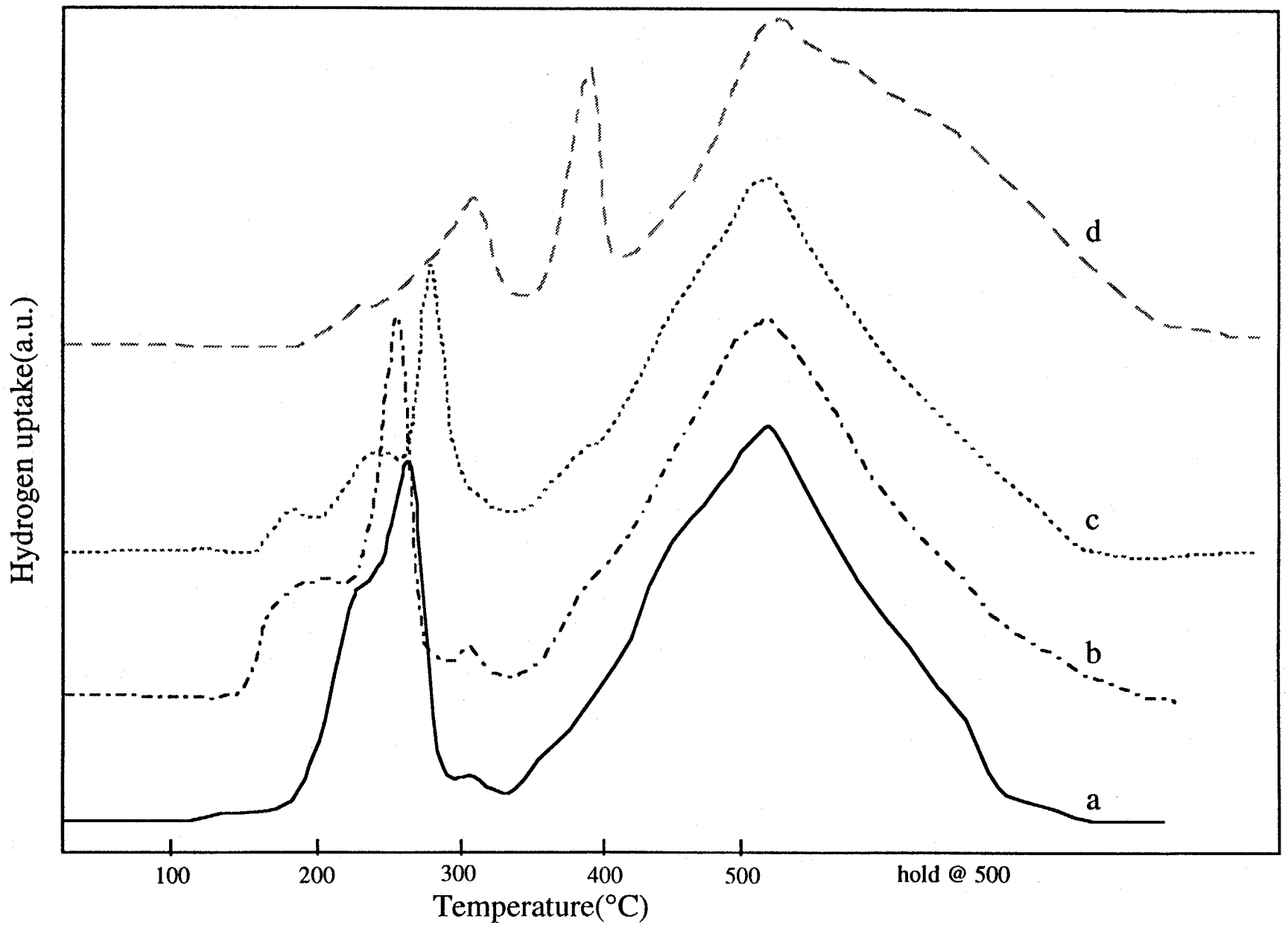

Fig. 6 `H_2-TPR results of UCI iron catalyst(1185-149) after preconditioning in argon flow
a. 150°C x 2 hours, b. 430°C x 1hour, c. 500°C x 1hour , d. 2nd-run H_2-TPR

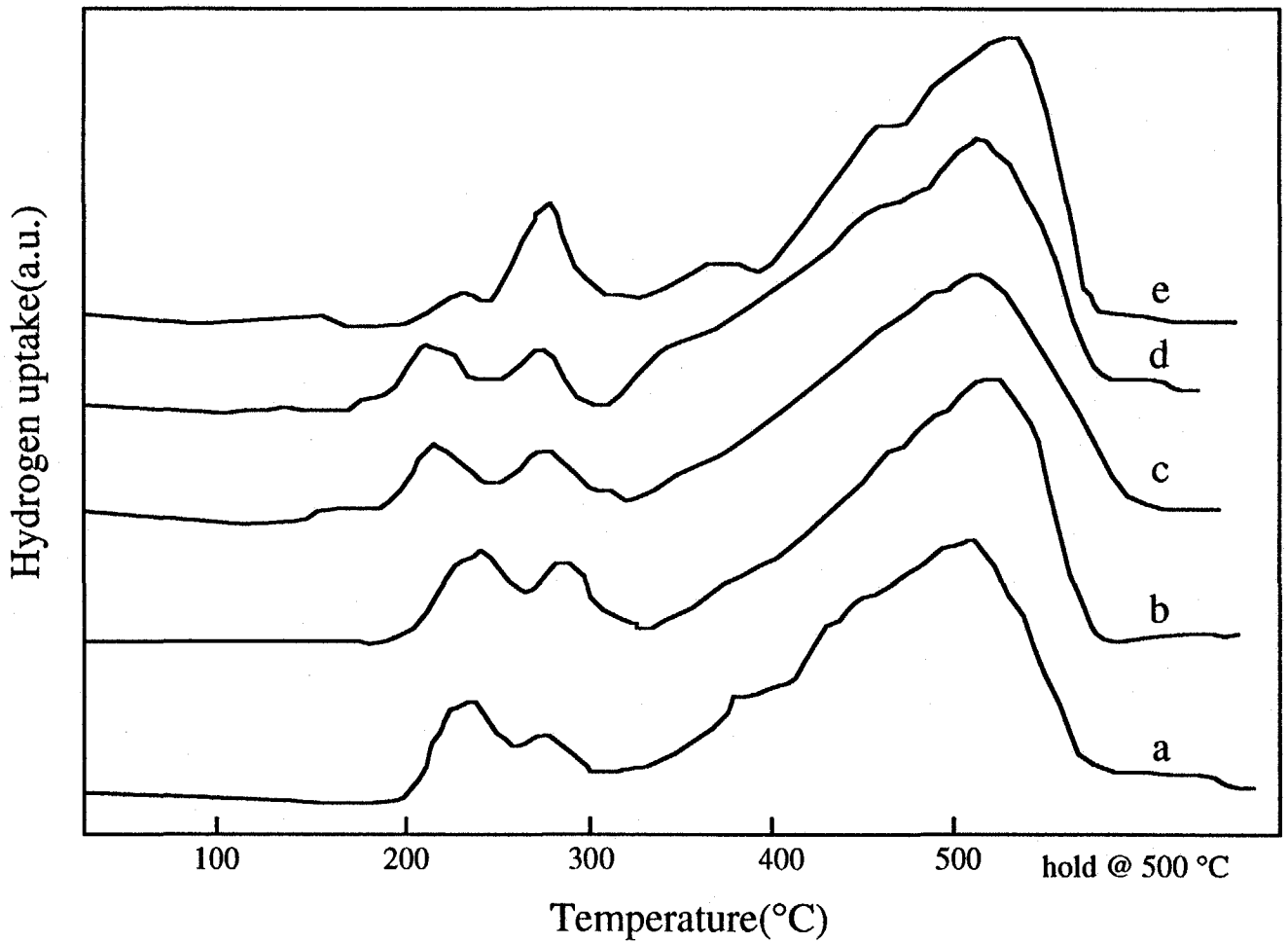

Fig. 7 H_2-TPR of YJ/1-65A(20 wt% Fe on silica sphere) after preconditioning in an argon flow
a. without preconditioning, b. 150°C x 2 hours, c. 430°C x 1hour,
d. 500°C x 1 hour, e. 2nd-run TPR

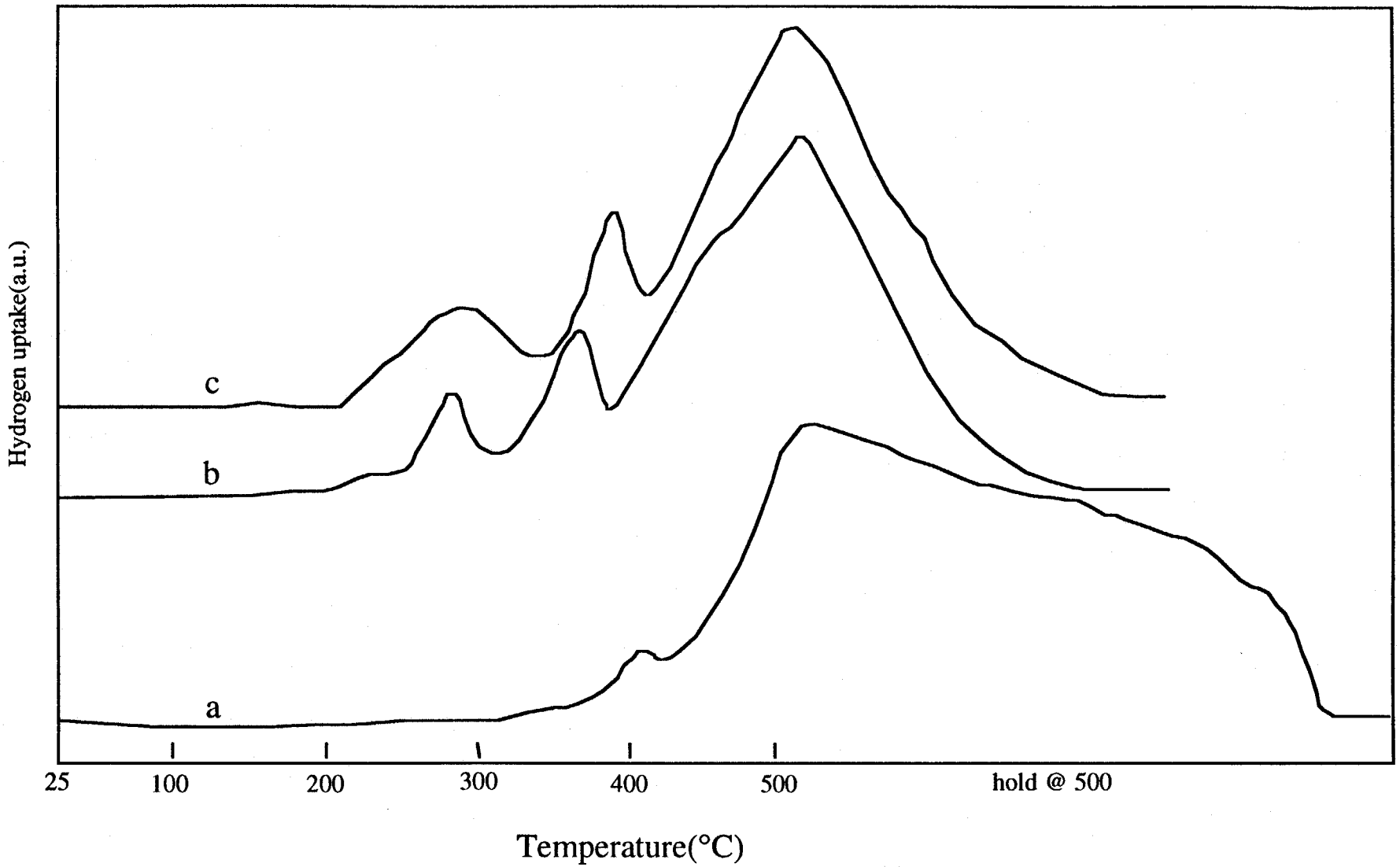

Fig.8. H_2-TPR of reference samples after preconditioning at 430°C for 1 hour
a. commercial magnetite, b. physical mixture of UCI 1185-149(50 wt%) and silica sphere
c. 2nd-run TPR of b

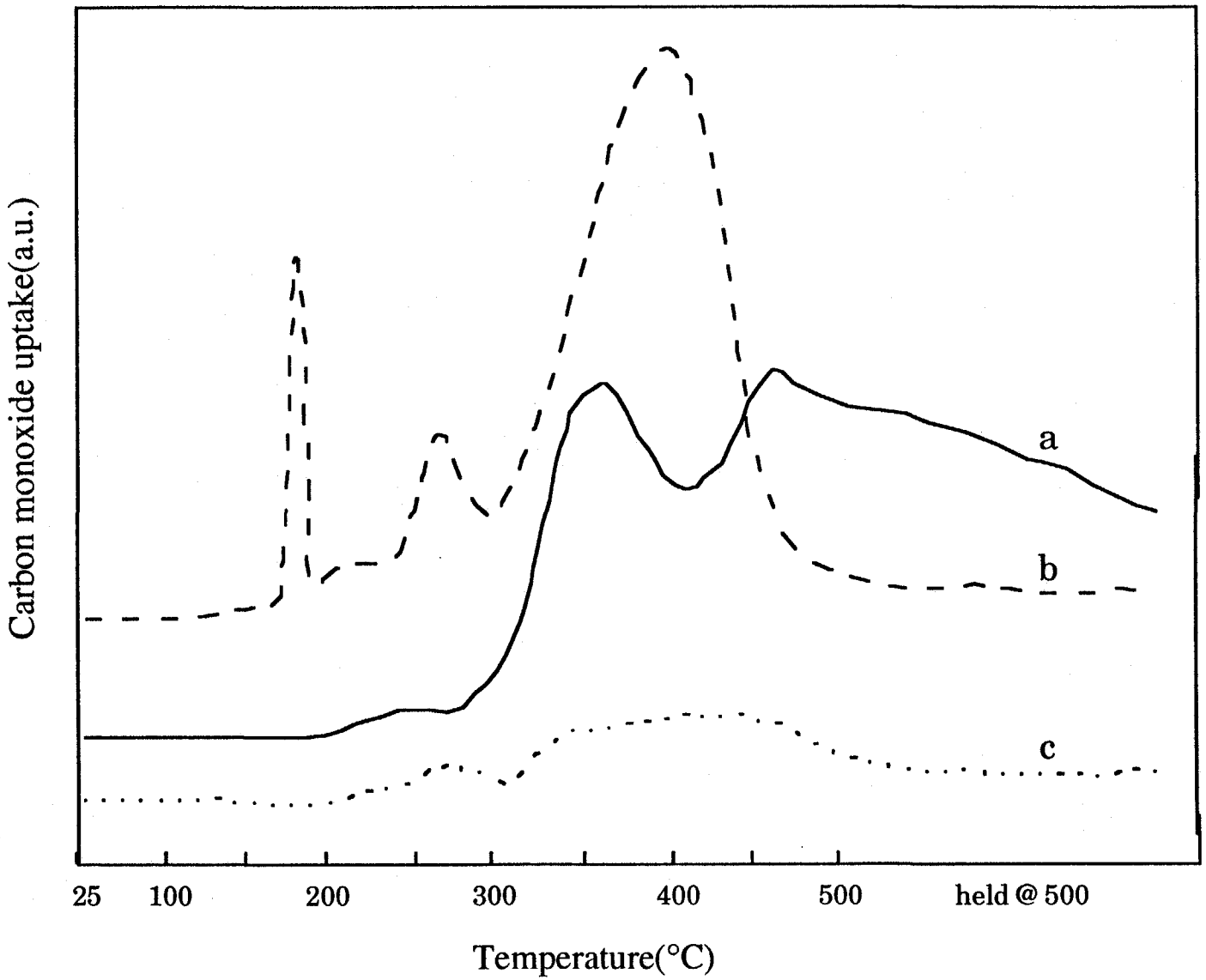

Fig.9. 1st-run CO-TPR results of iron catalysts

a. YJ/1-65A, b. UCI iron catalyst(1185-149), c. YJ/1-67(10 wt% Fe on silica sphere)

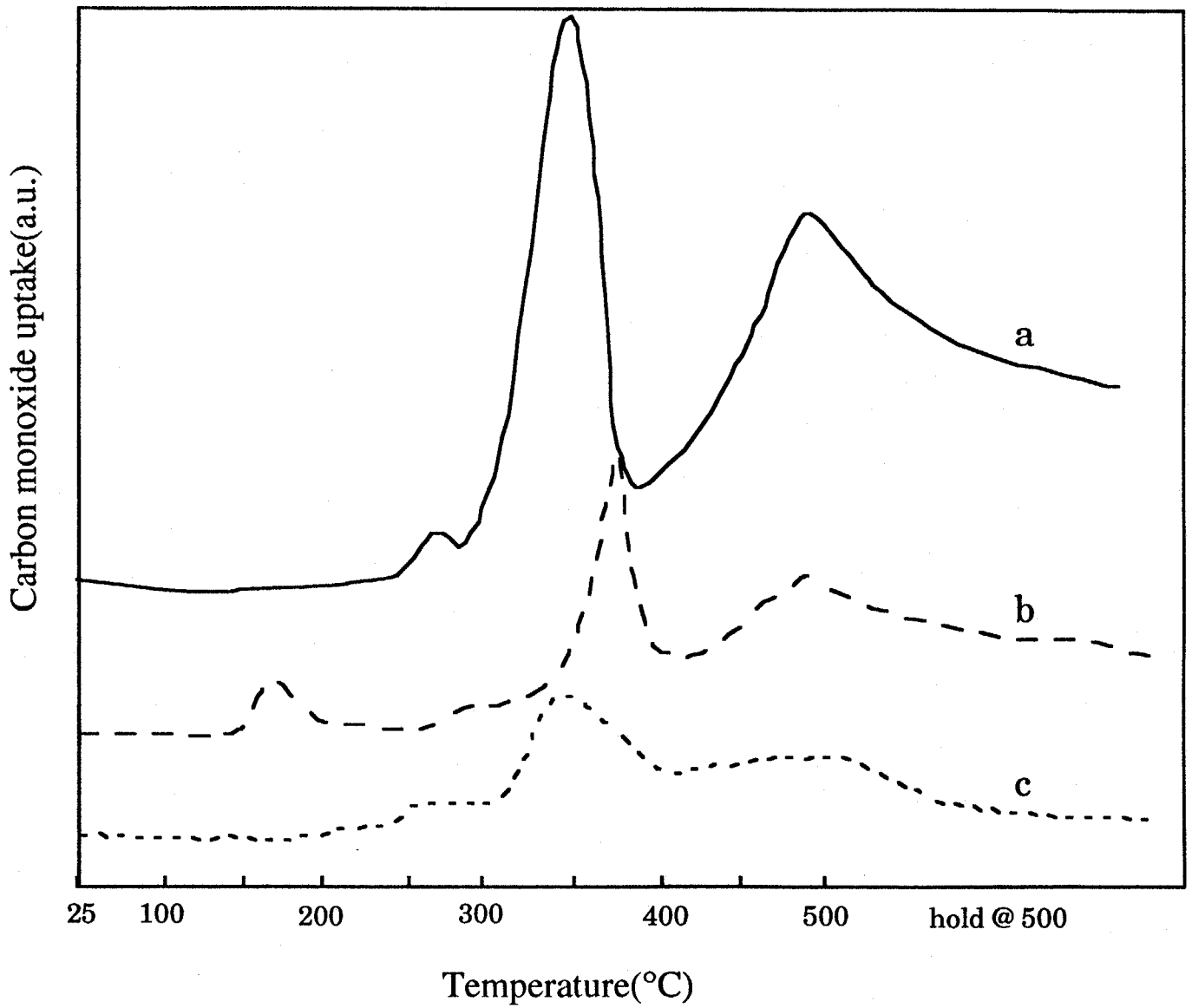

Fig. 10. 2nd -run CO-TPR results of iron catalysts

a. YJ/1-65A, b UCI catalyst, c. YJ/1-67

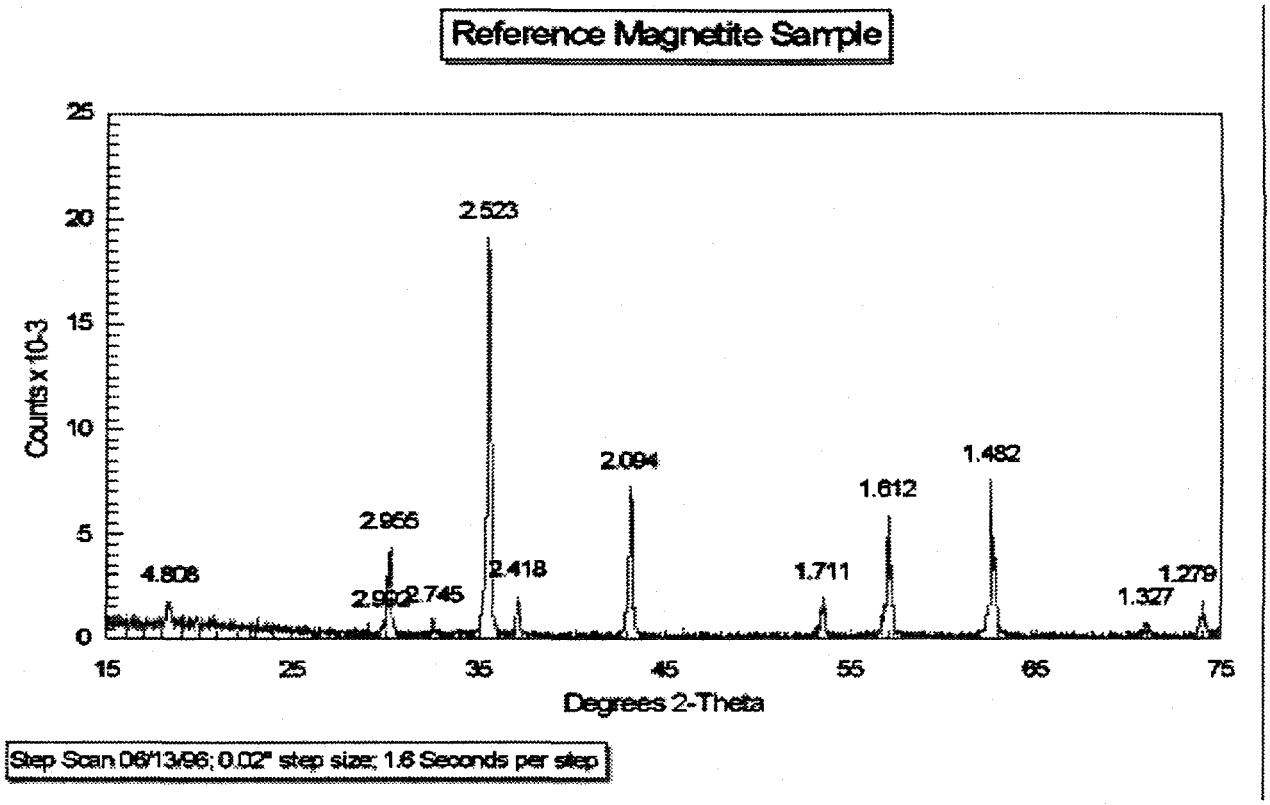

Figure 11. XRD pattern of natural magnetite

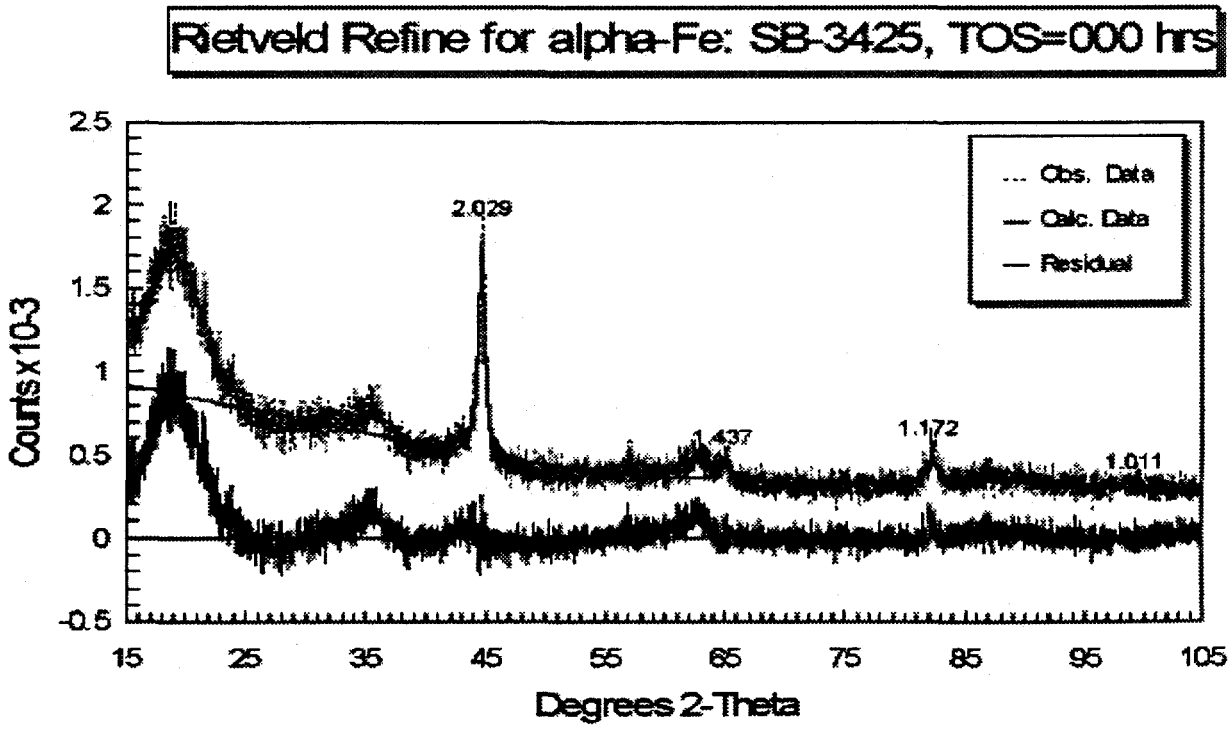

Fig. 12 XRD powder pattern of TAMU catalyst sample at time on stream = 0 hrs. Reitveld refinement shows that the primary constituent is α– Fe.

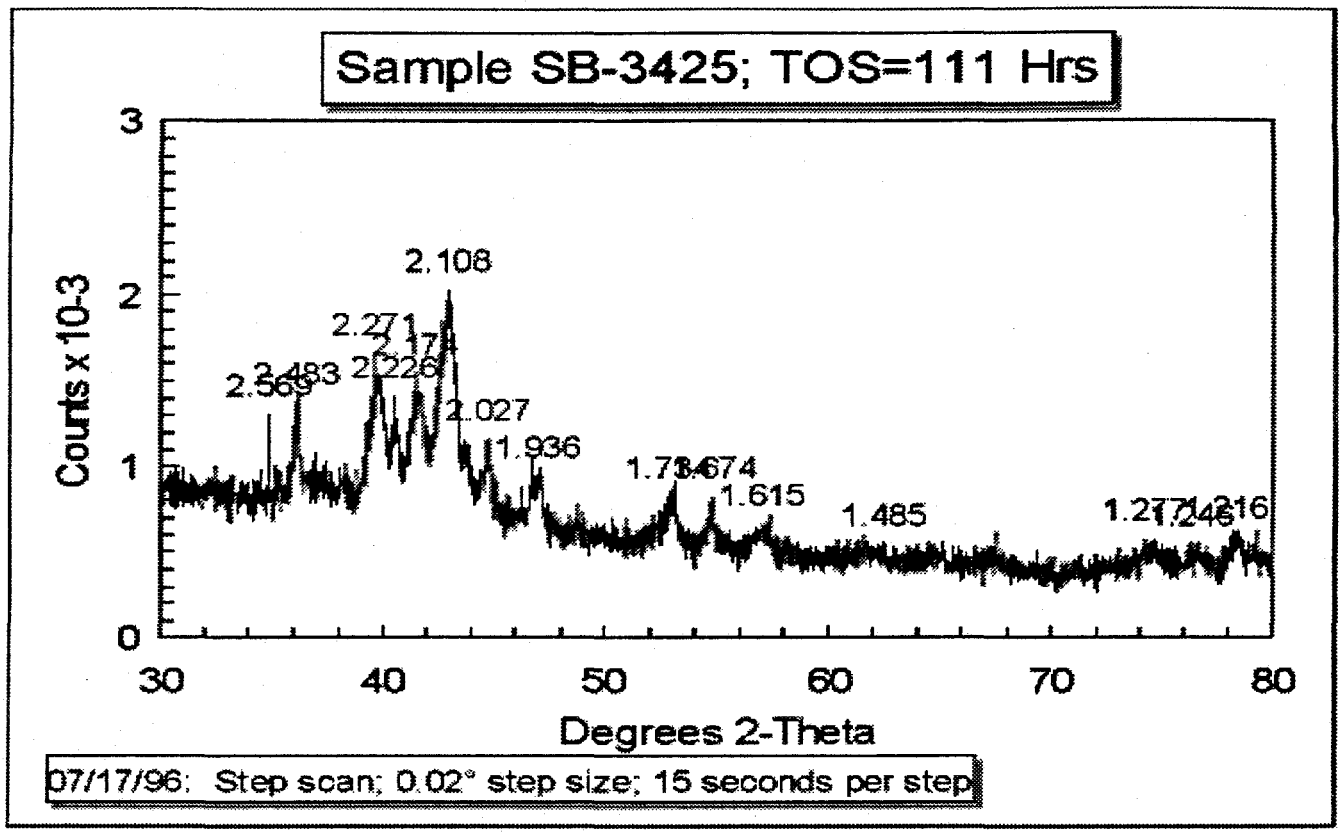

Figure 13 Sample of catalyst from run SB-3425 after 111 hours on stream. The prominent peaks can be attributed to the carbide phase. By analyzing the sample in wax, we prevent surface oxidation which occurs when the wax is stripped off.

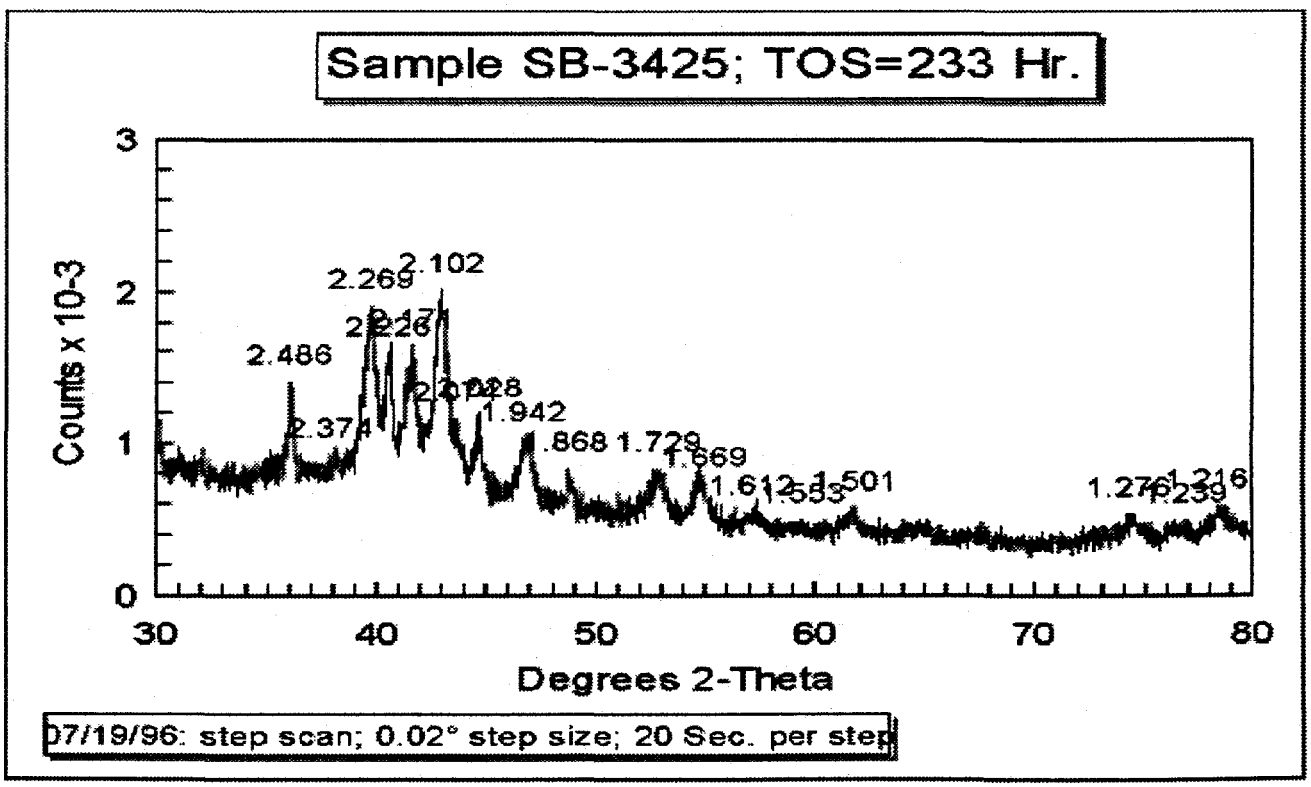

Figure 14 After 233 hours on stream, the carbide peaks grow in height indicating that the crystallinity of the sample has increased.

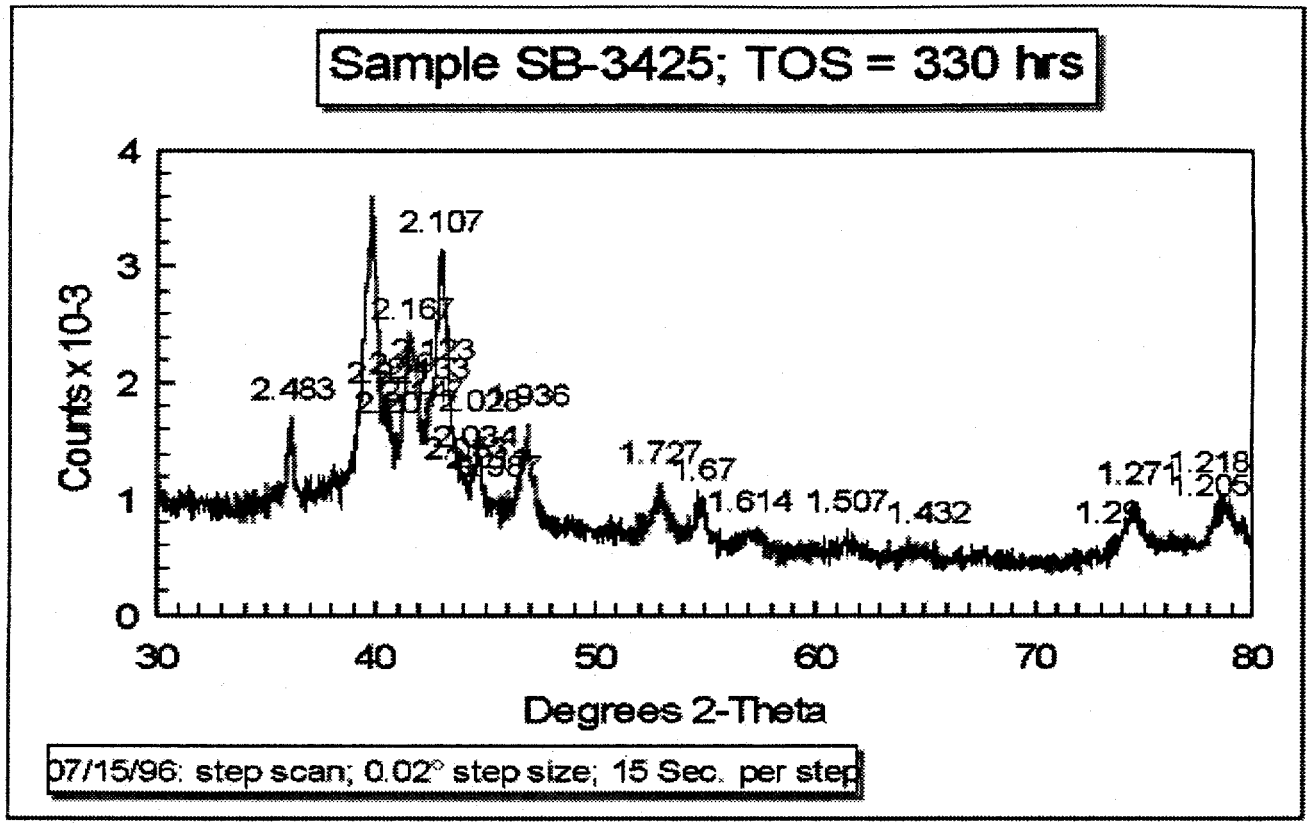

Figure 15 XRD pattern of catalyst after 330 hours on stream. The increased crystallinity of the carbide is seen in the growth of these peaks. There appears to be no transformation of carbide into magnetite.

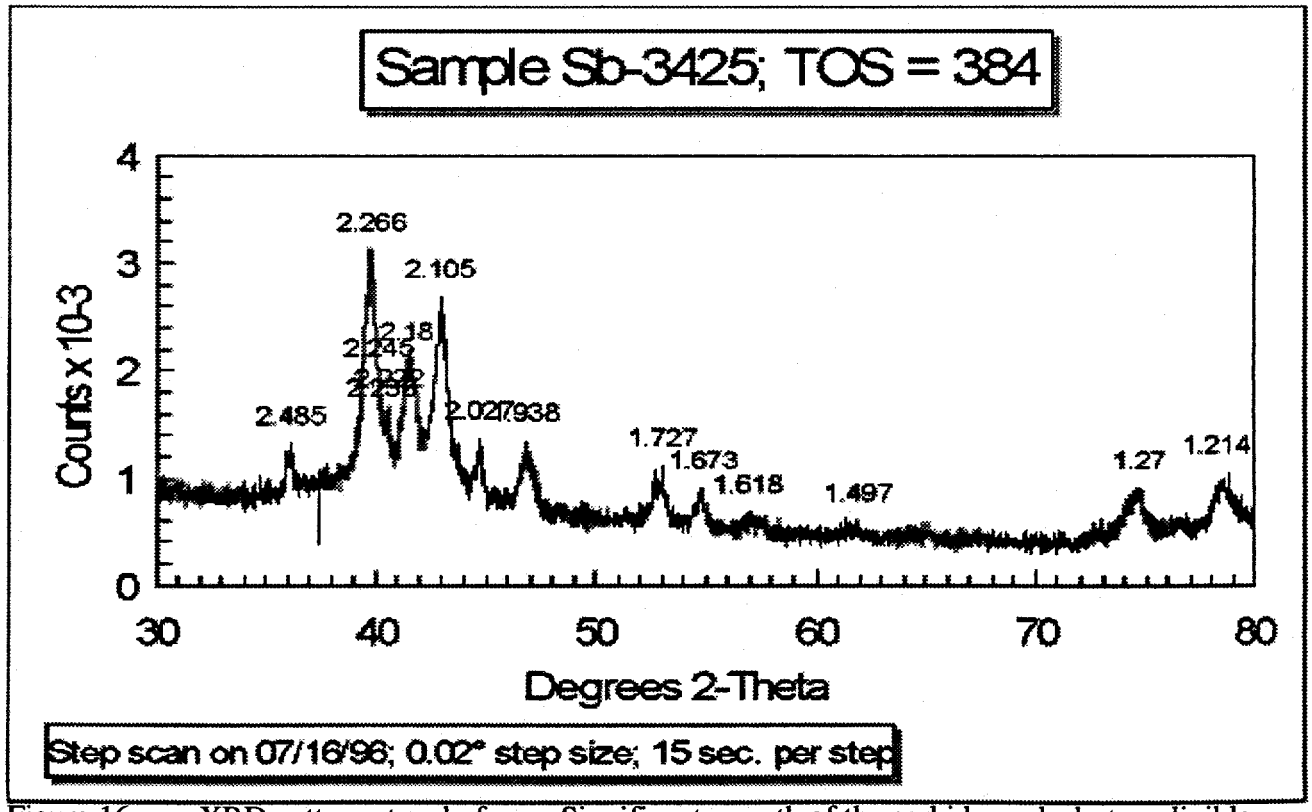

Figure 16 XRD pattern at end of run. Significant growth of the carbide peaks but negligible amounts of the magnetite phase seen over the course of this run.

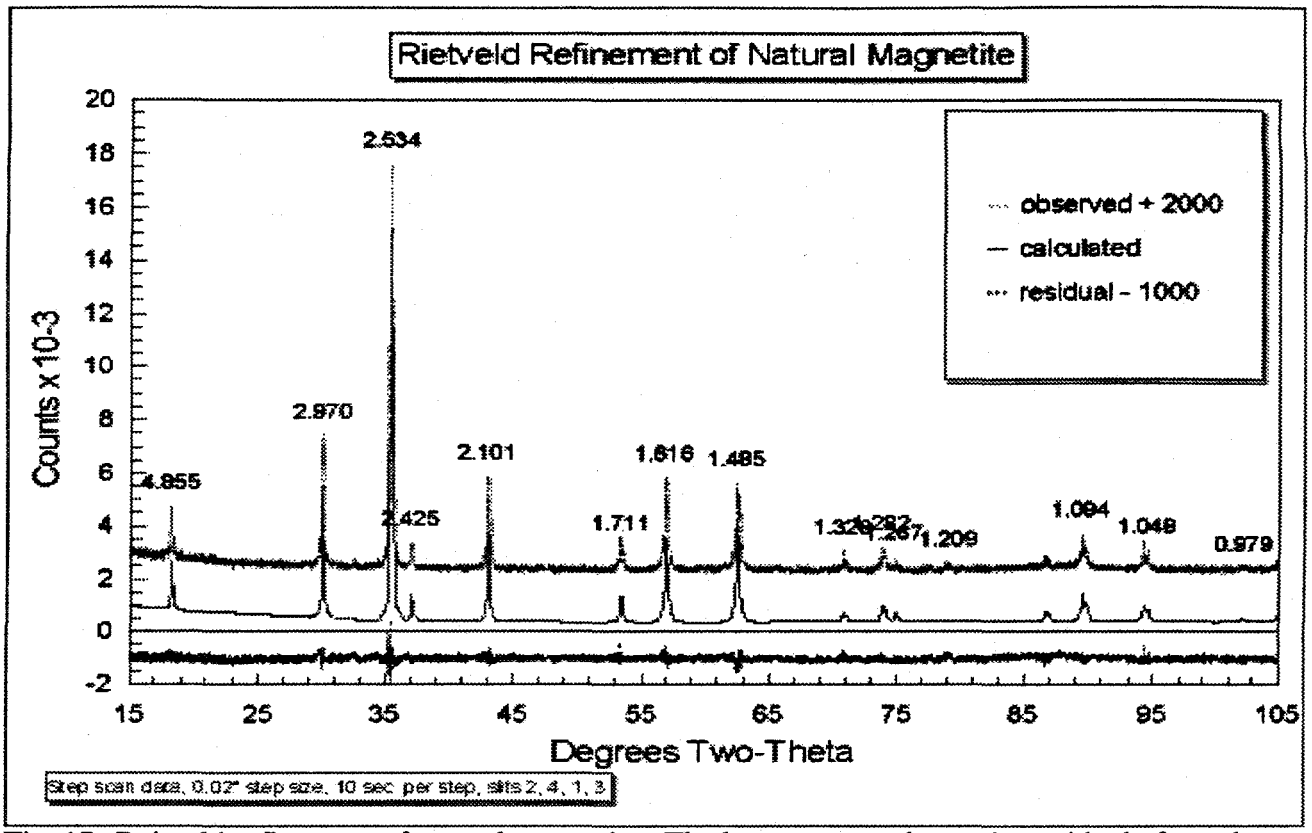

Fig. 17 Reitveld refinement of natural magnetite. The lowest curve shows the residual after subtracting the calculated pattern from the experimental one. It shows that the Reitveld method provides an excellent fit to the experimental data, accounting correctly for the intensities of the various peaks

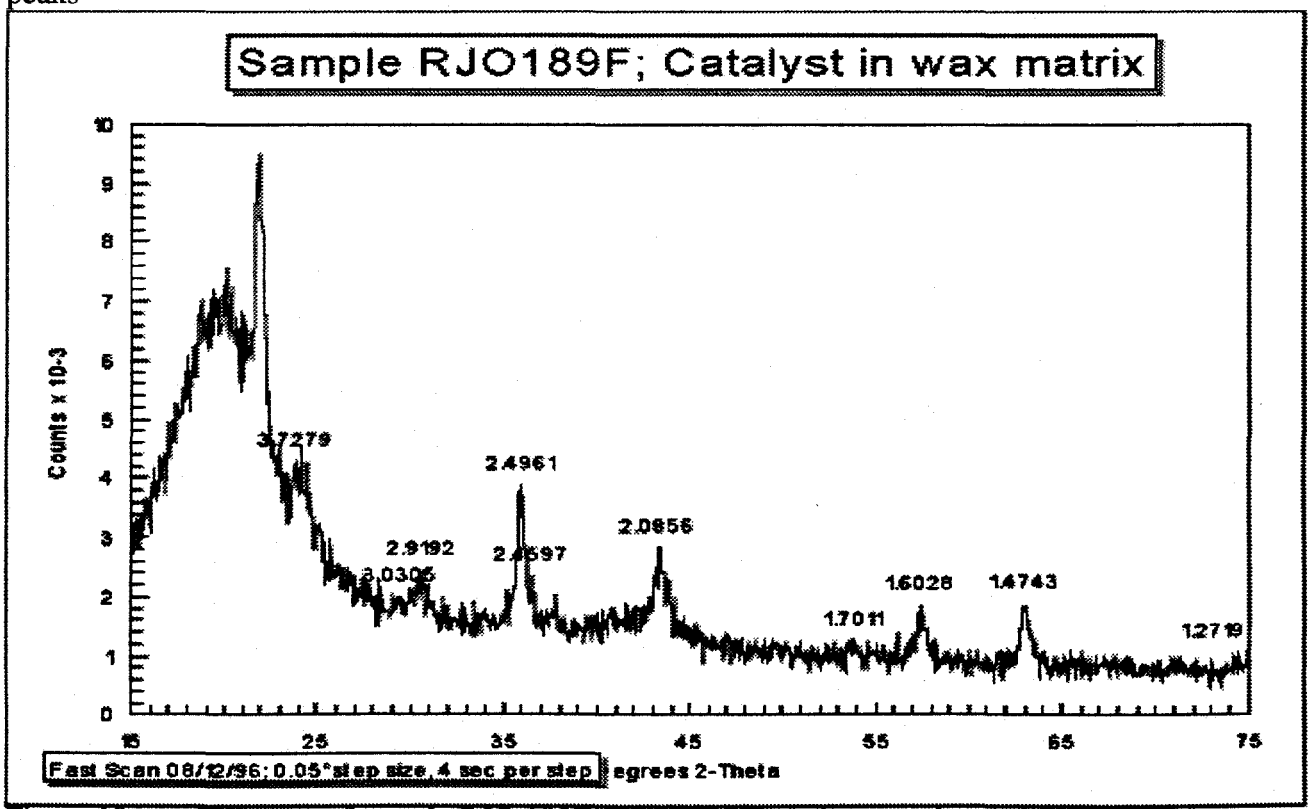

Figure 18 Fast scan of sample RJO 189F (TOS 20h. Prominent peak corresponding to magnetite is seen at 2.496 Å. However the size of the 2.0856 peak suggests the presence of carbide as well.

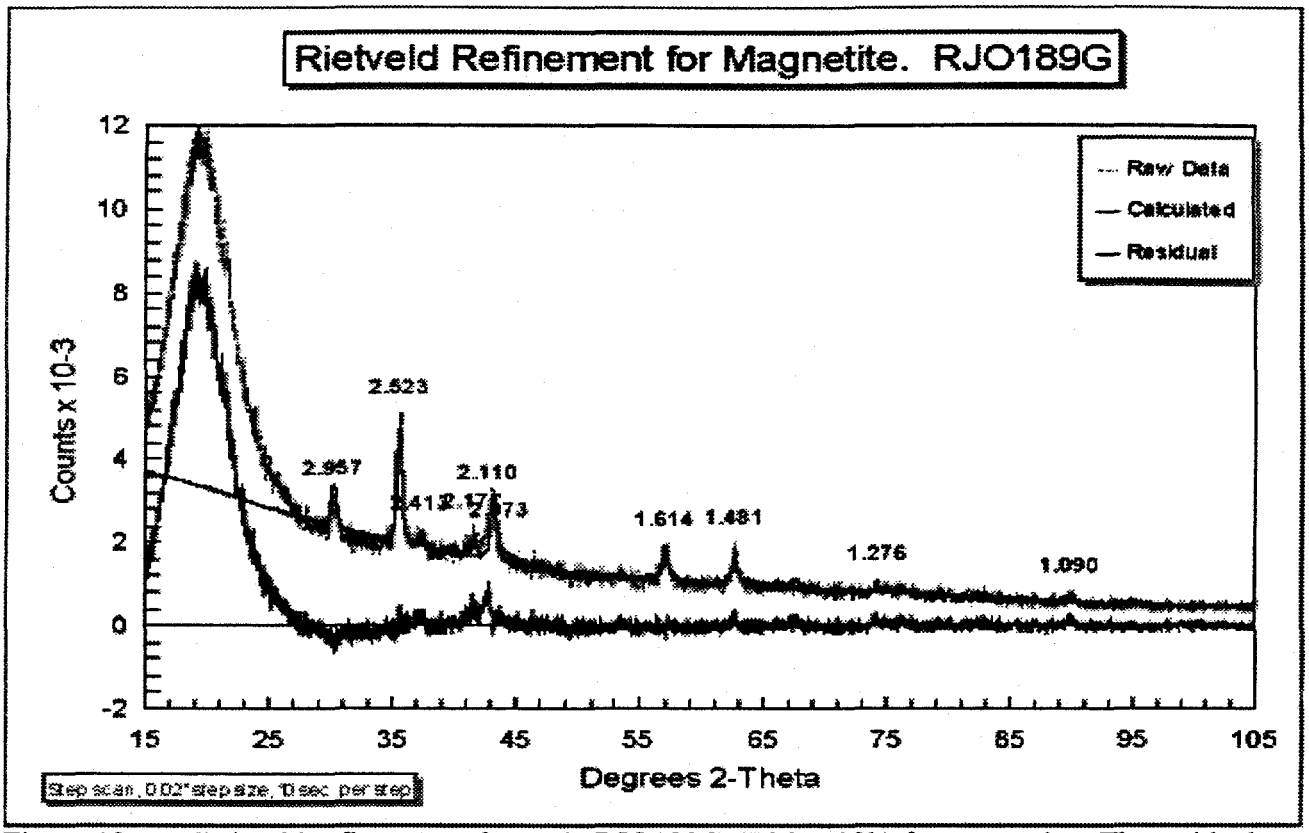

Figure 19 Reitveld refinement of sample RJO189G (TOS=122h) for magnetite. The residual after subtraction of magnetite is a a small peak corresponding to iron carbideas shown below.

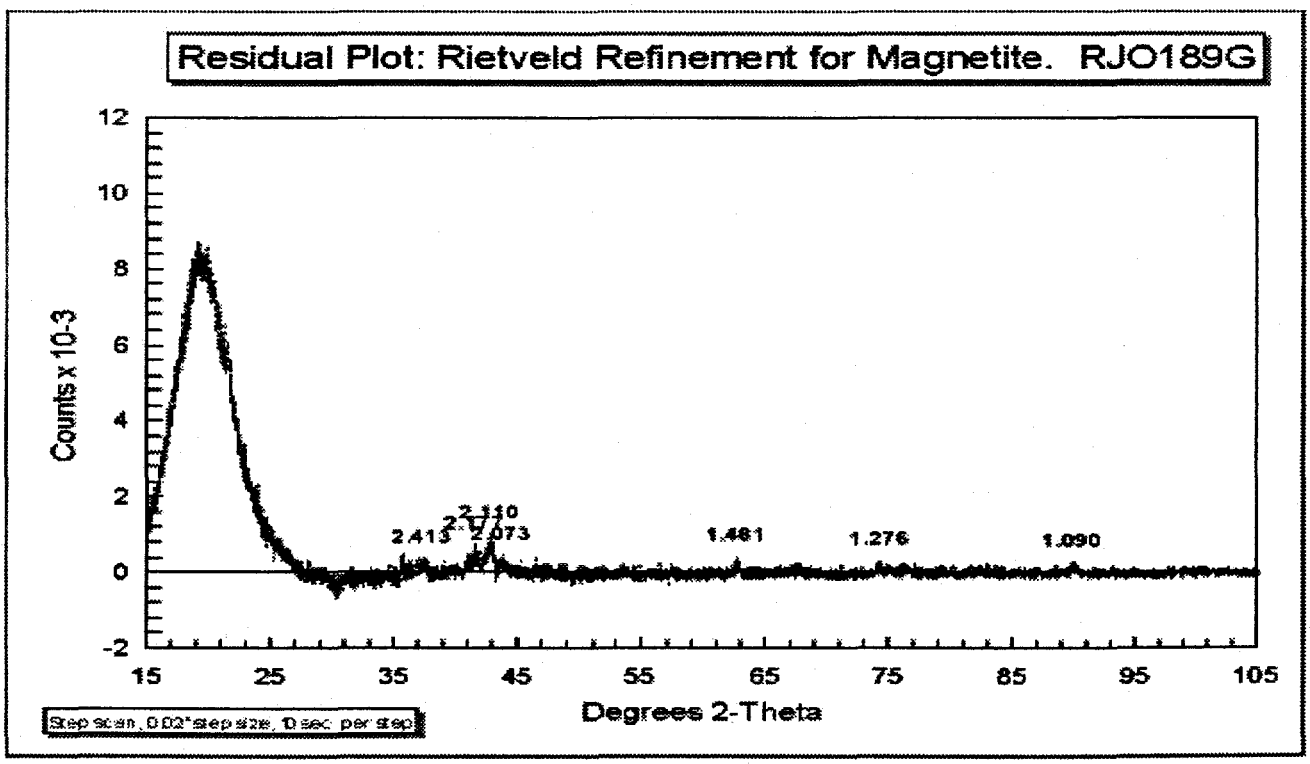

Figure 20 Residual after subtracting magnetite from the XRD powder pattern of sample RJO 189G

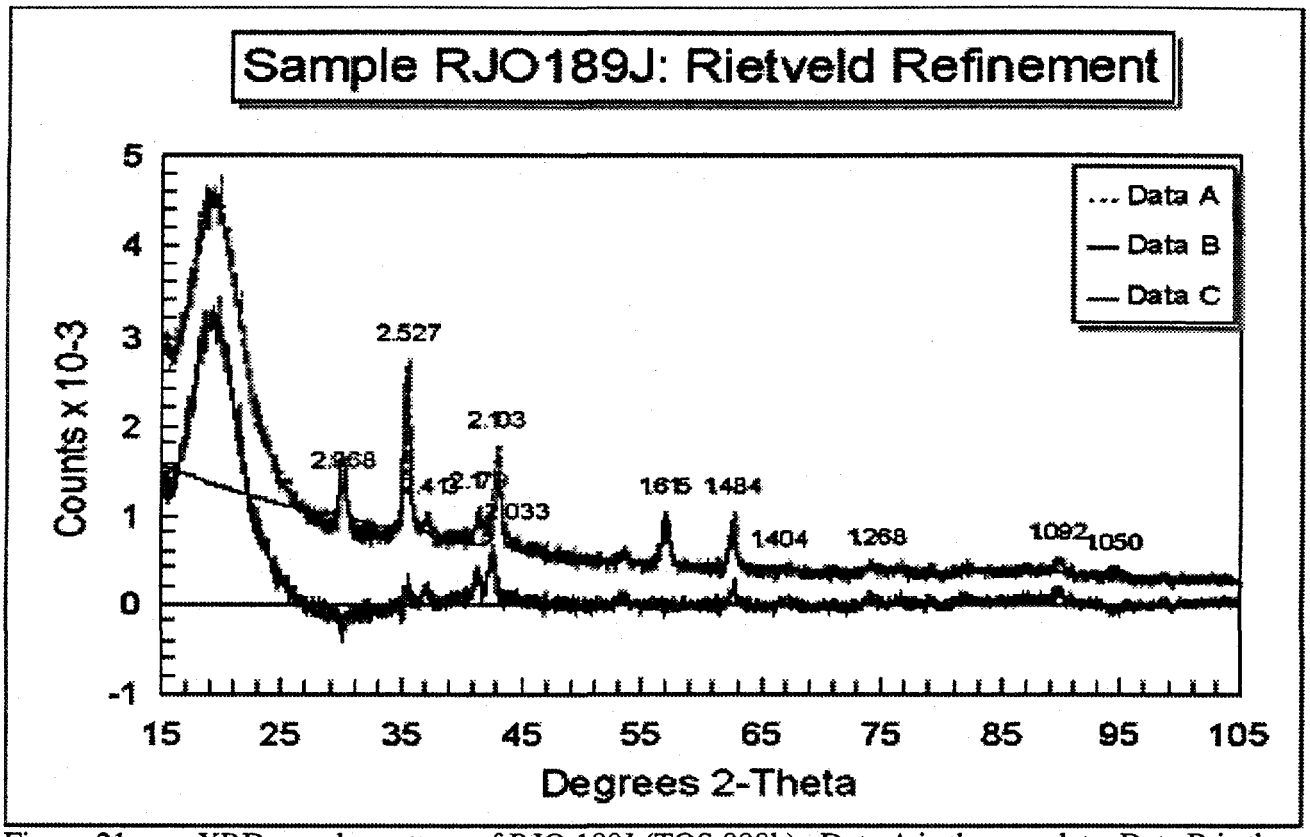

Figure 21 XRD powder pattern of RJO 189J (TOS 888h). Data A is the raw data, Data B is the refined pattern for magnetite and Data C is the residual.

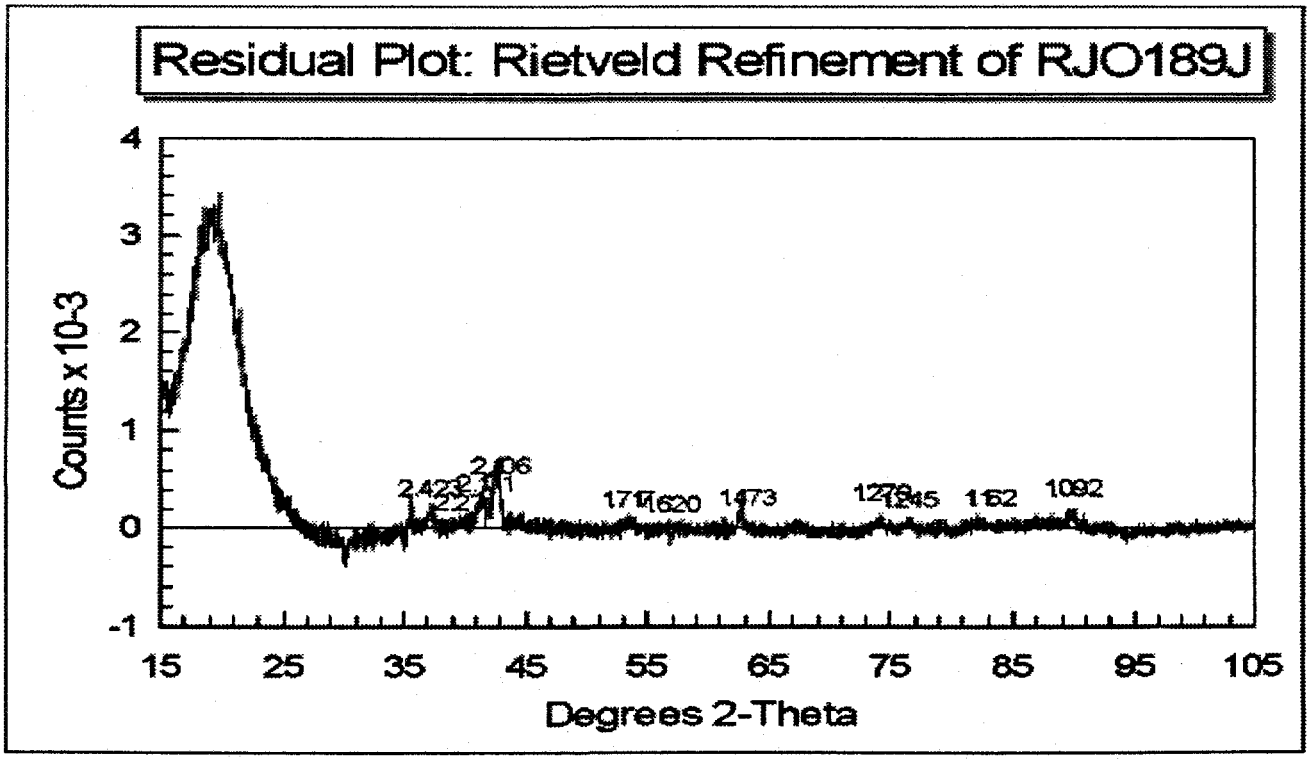

Figure 22 The residual after subtracting magnetite shows peaks corresponding to iron carbide.

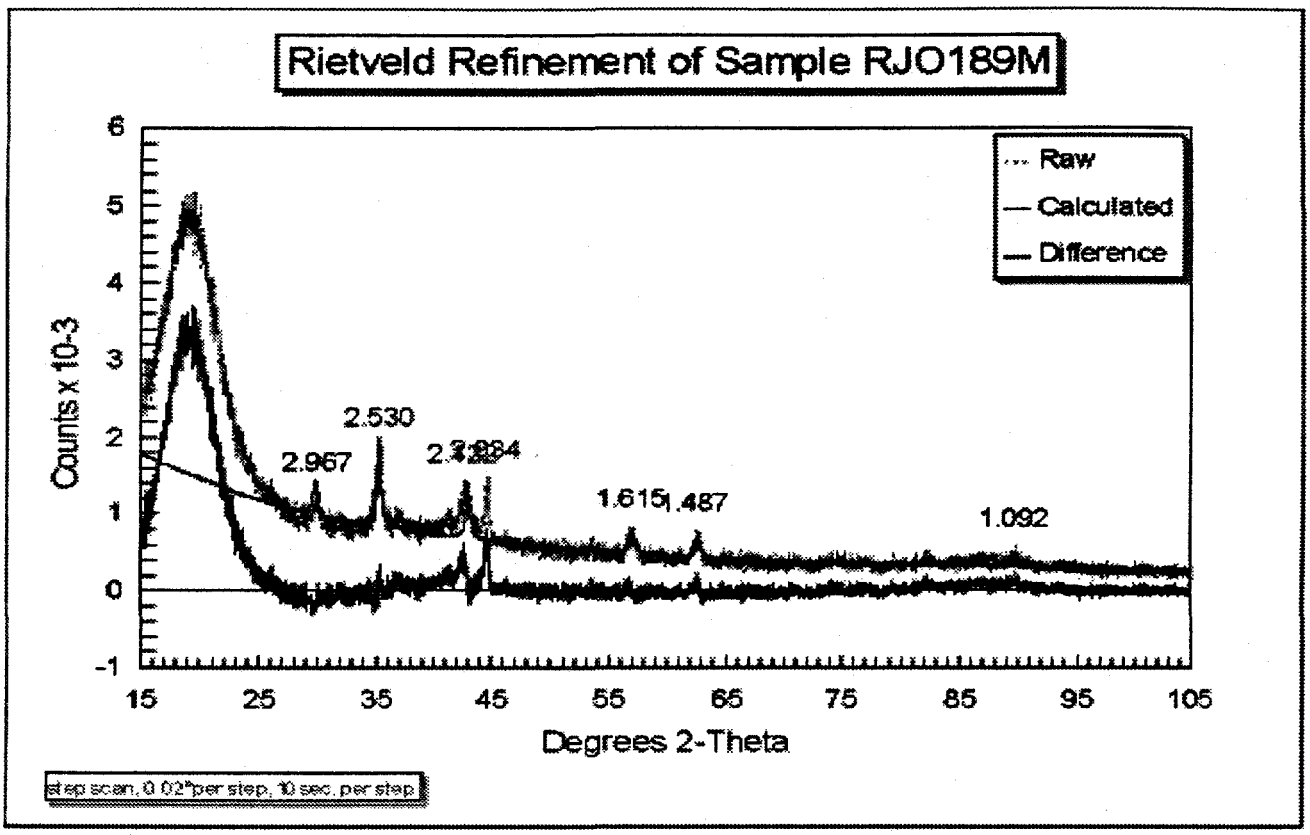

Figure 23 XRD powder pattern of sample RJO189 M showing how the Reitveld refinement for magnetite leaves behind a two peak pattern.

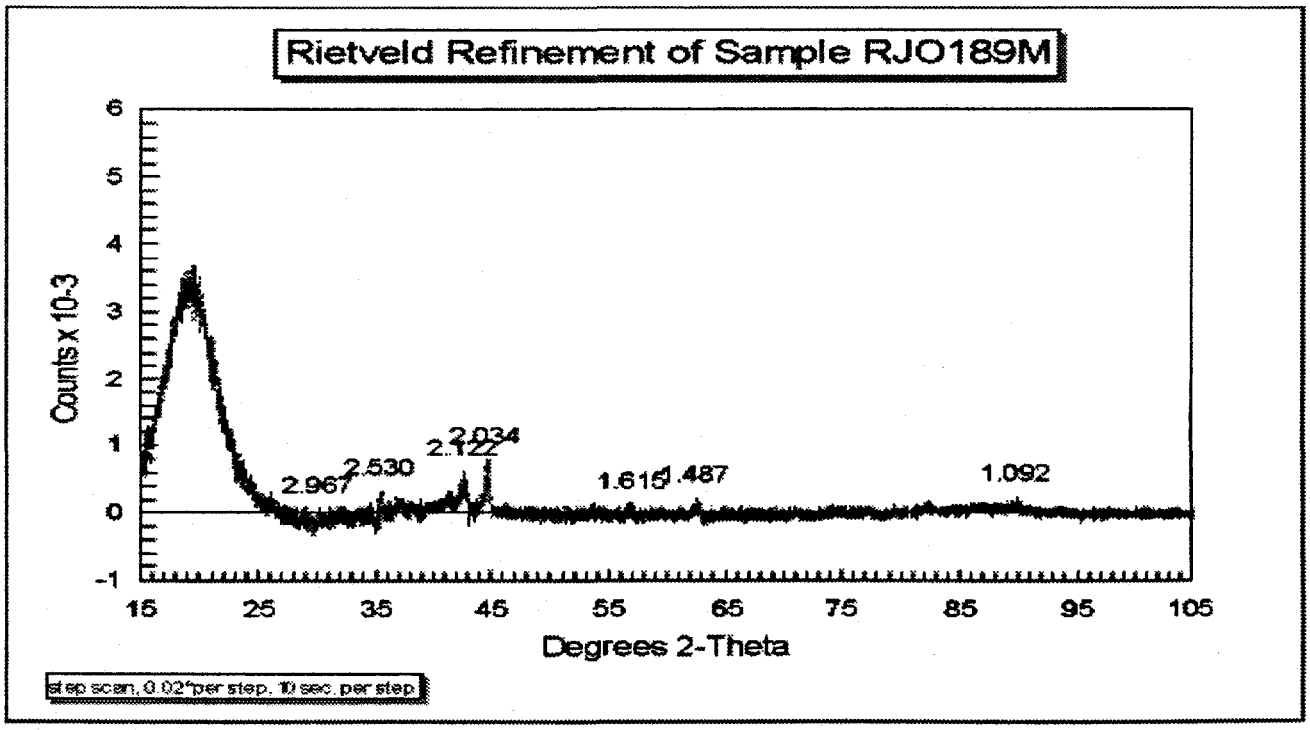

Figure 24 The residual from sample RJO 189M (TOS 1796h) shows two prominent peaks after the magnetite has been subtracted.

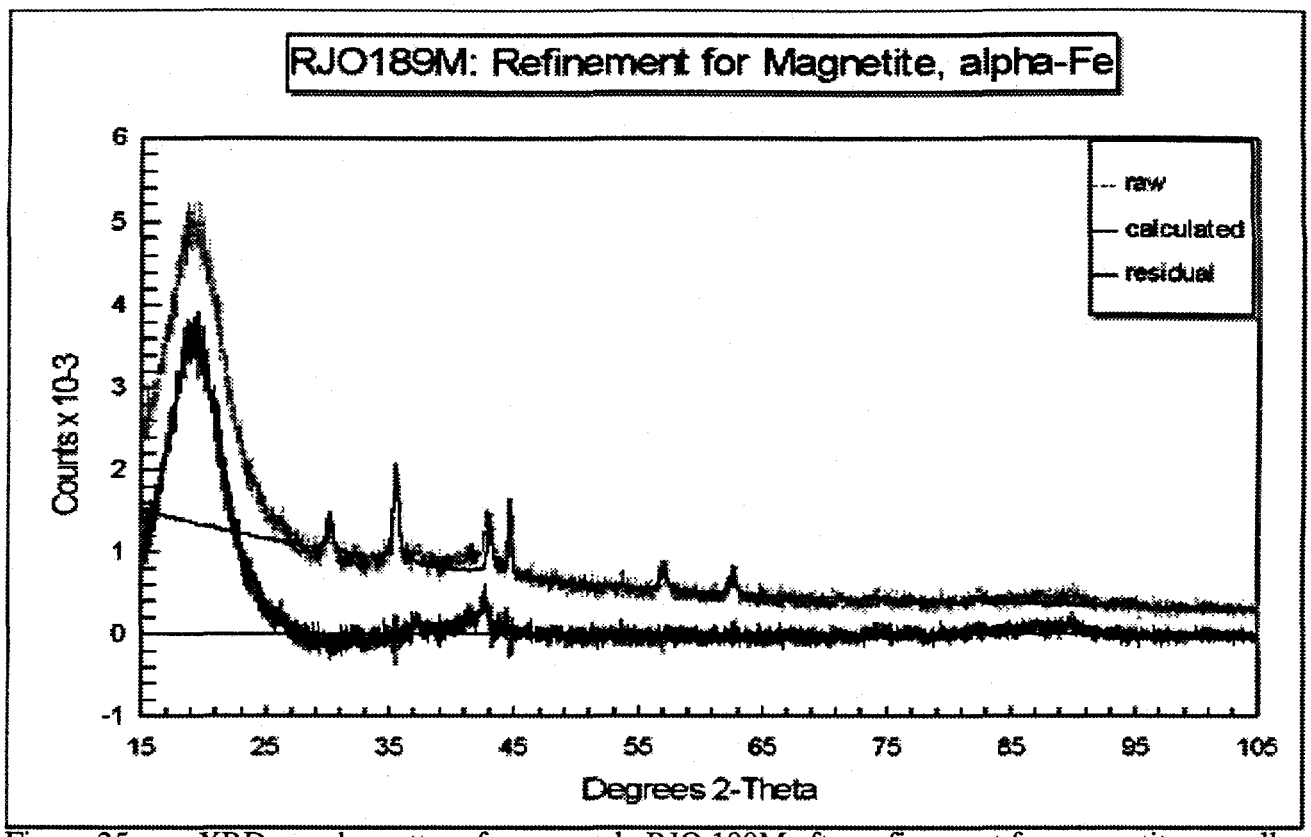

Figure 25 XRD powder pattern from sample RJO 189M after refinement for magnetite as well as α– Fe. The residual now shows peaks attributable to iron carbide.

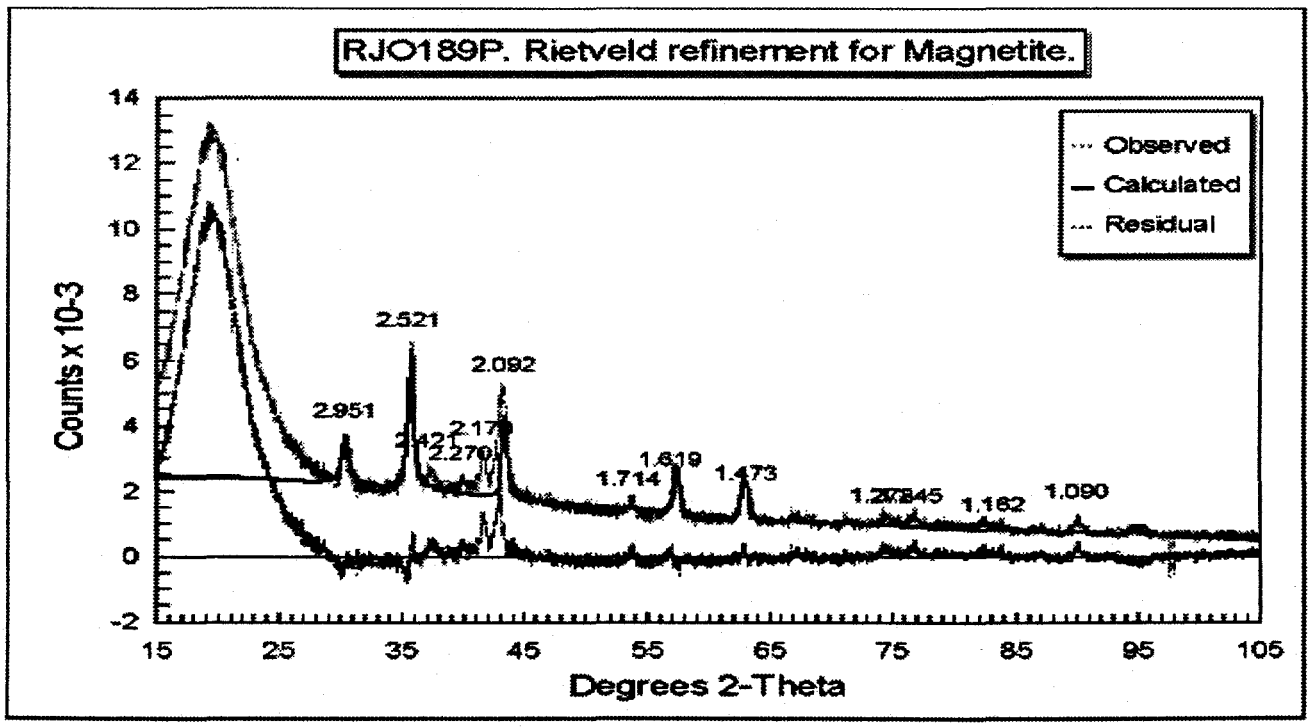

Figure 26 XRD powder pattern from sample RJO 189P (TOS = 3547h) after Reitveld refinement for magnetite.

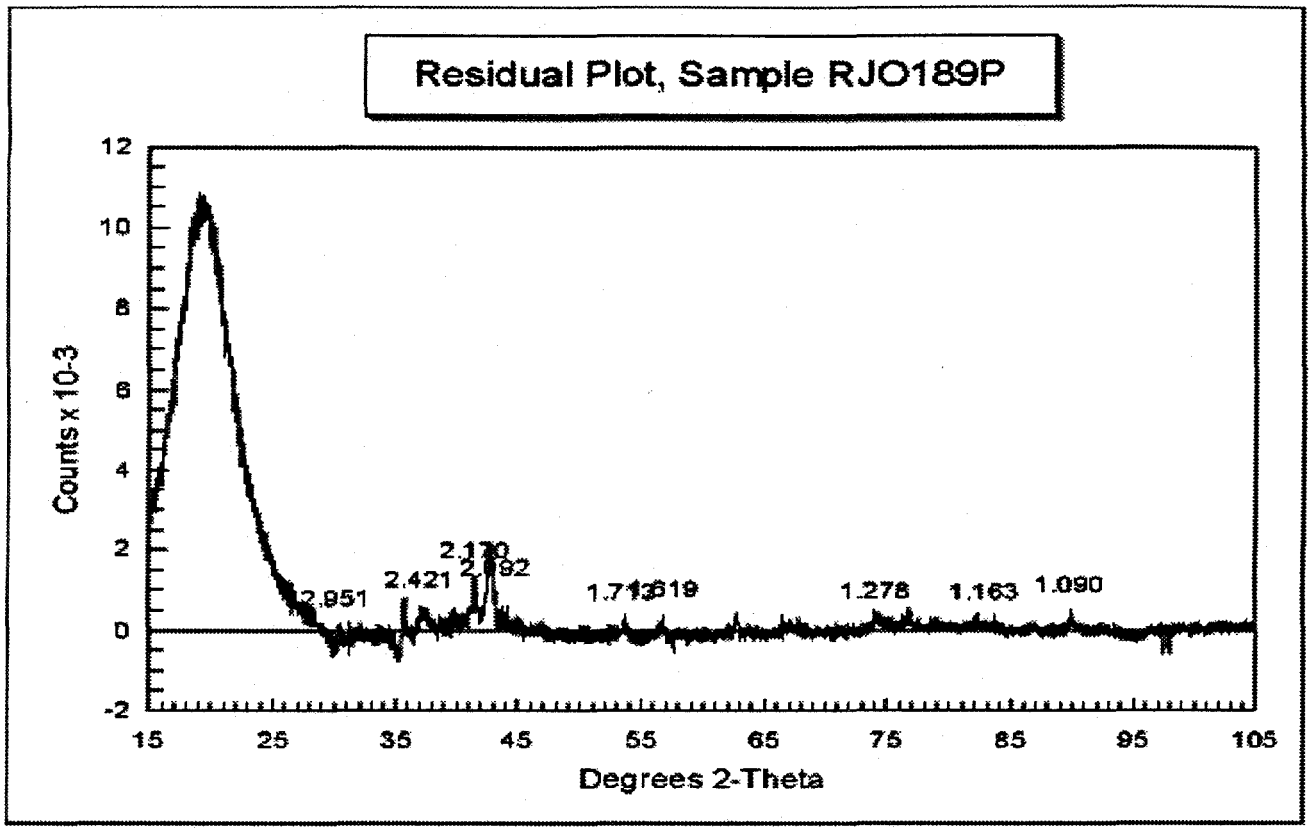

Figure 27 Residual plot from sample RJO 189P (TOS = 3547 h) after subtracting the magnetite peaks. A two peak pattern is seen, however the second peak does not match that for α– Fe.

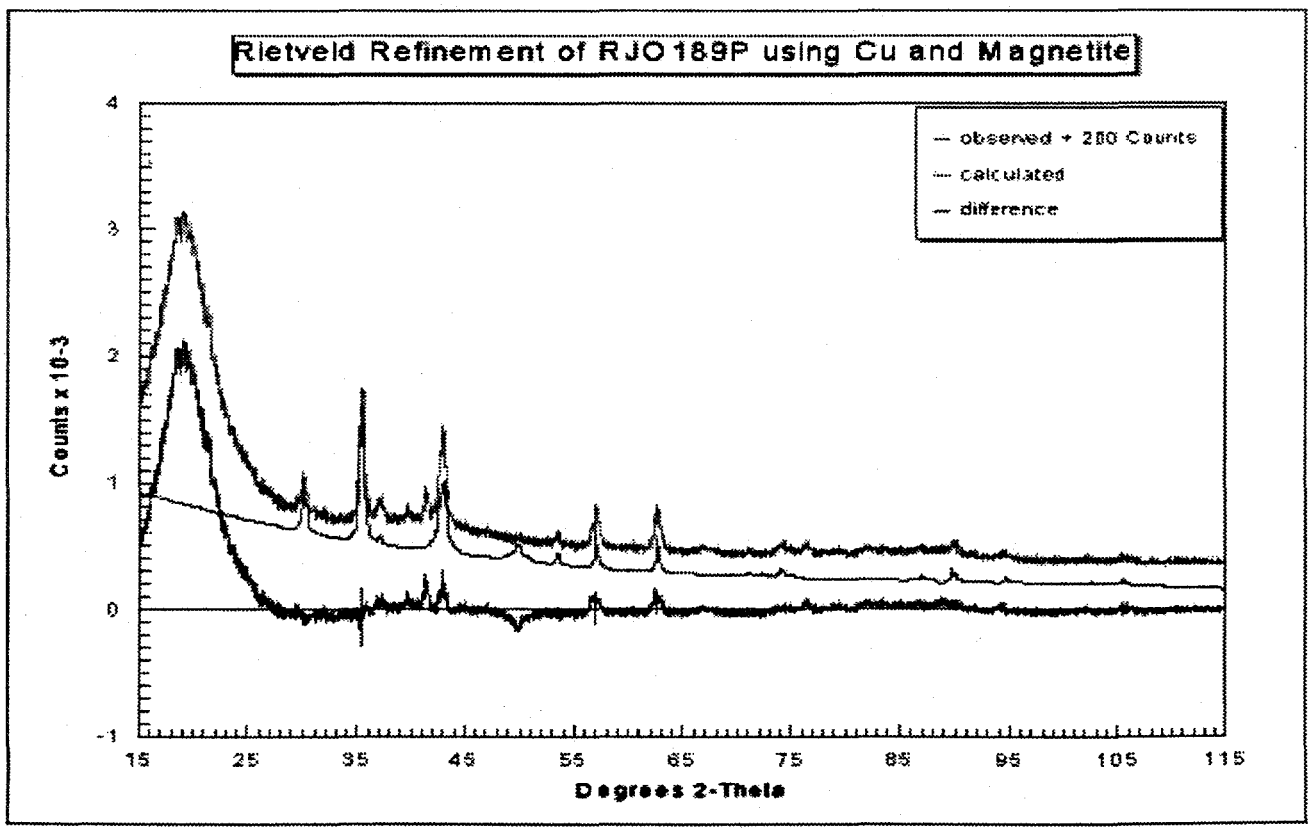

Figure 28 A trial fit was performed for metallic Cu, however, as shown here, subtraction of Cu yielded negative peaks in the residual showing that free Cu was not present in this sample.